Modeling of Anomalous Transport in ECRH Plasmas at HSX

W. Guttenfelder[1], D.T. Anderson[1], J.M. Canik[1], K.M. Likin[1], J. Lore[1], J.N. Talmadge[1], W. Dorland[2], M. Barnes[2]

[1] *University of Wisconsin, Madison, USA*

[2] *University of Maryland, USA*

The gyrokinetic code GS2 has been used to calculate the linear growth rates of the underlying micro-instabilities presumably responsible for the anomalous transport in HSX. With ECRH heating ($T_e >> T_i$), the dominant long-wavelength instability is the trapped electron mode (TEM). To test whether available TEM transport models can reproduce the transport in HSX, the Weiland ITG/TEM transport model is used, in addition to calculations of neoclassical transport, to predict plasma profiles in HSX. To approximate the 3D geometry of HSX in the Weiland model, the necessary input geometry information is taken from the region in HSX where the fastest growing modes are spatially localized in the 3D GS2 calculations. Specifically, the local curvature/∇B scale lengths (~R/3) and helical ripple (ε_H) are used in place of the axisymmetric values (R and ε_T = r/R, respectively). With these approximations, the TEM linear growth rates predicted by the Weiland model agree quantitatively (within 30%) with those predicted by the 3D GS2 calculations for HSX experimental parameters. Predicted density and temperature profiles using the above transport estimates are in reasonable quantitative agreement with a number of experimental profiles in the QHS configuration. The predicted confinement times are within ~10% of the experimental confinement times.

Keywords: turbulent transport model, quasi-linear transport, 3D gyrokinetic stability, trapped electron mode

1. Introduction

It has become routine to optimize stellarators using neoclassical theory [1]. It is hoped that in the future, stellarators may also be optimized to reduce anomalous transport, thought to be caused by plasma turbulence. Indeed, there is evidence in LHD that anomalous transport is reduced when neoclassical transport is reduced [2]. While significant advances have been made in the predictive capability for turbulent transport in tokamaks [3], relatively little work has been performed for 3D toroidal configurations such as stellarators.

Turbulent transport in tokamaks (caused by drift waves) has been modeled through the use of quasi-linear transport estimates that have been scaled to match non-linear simulations [4-6]. Suppression of turbulent transport via equilibrium E×B shear has also been included to successfully model H-mode pedestals and internal transport barriers [7]. These two features appear to provide the dominant scaling in predicting turbulent transport (via drift waves) in tokamak plasma.

Measured turbulence characteristics [8] and energy confinement time scaling [9] are quite similar in tokamaks and stellarators. Furthermore, recent non-linear simulations [10,11] have demonstrated that predicted turbulence characteristics in stellarator geometries display similarity to those predicted in tokamaks. However, because of the 3D shaping, stellarator non-linear simulations require increased resolution to treat the non-symmetric geometry and various classes of trapped particles, and are therefore more computationally expensive.

Given the similarity in turbulence and energy confinement between stellarators and tokamaks, a logical first step in performing predictive transport modeling for present stellarator experiments is to follow the same framework as used for tokamak predictions. Following this reasoning, this paper will present predictions of density and temperature profiles in the HSX stellarator using a tokamak transport model. To justify the use of this model for the 3D geometry in HSX, comparisons will be made between linear growth rates predicted by the tokamak model, and those calculated using a 3D gyrokinetic code that uses the HSX equilibrium.

2. 3D Gyrokinetic Microstability Calculations

The initial value gyrokinetic code GS2 [12] has been previously used to calculate linear micro-stability in a stellarator configuration [13]. To perform these

author's e-mail: guttenfe@cae.wisc.edu

calculations, 3D equilibrium are calculated using VMEC [14,15], which are then transformed into Boozer coordinates using TERPSICHORE [16]. GS2 uses a ballooning representation, and the necessary geometry coefficients along a field line are calculated using VVBAL [17]. Since stellarators in general have multiple ripples in |B| along a field line, care must be taken in creating a grid that captures these additional non-symmetric ripples. Multiple grids have been created for the quasihelically symmetric (QHS) configuration of HSX with varying number of grid points to determine how well these additional ripples must be resolved to reach a converged solution. For the calculations shown in this paper, 400 grid points (over a range of $\theta = \pm 4\pi$) were sufficient. Typically 16 energy and ~30 pitch angle grid points were needed for the calculations to converge. To verify accuracy, a few cases were benchmarked against the independent linear gyrokinetic FULL code for the HSX geometry [18]. The GS2 calculations were performed on the NERSC IBM SP3 supercomputers using up to 256 processors, requiring a few minutes per run.

The linear stability calculations were performed on a field line where the magnetic axis undergoes the largest excursion to the outboard side, and hence has the strongest bad curvature drive. Figure 1 (top) shows eigenfunctions calculated for the QHS configuration for multiple poloidal wavenumbers ($k_\theta \rho_s$ = 0.3-0.8), at a normalized minor radius of ρ = 0.86, for experimentally relevant parameters (a/L_{Ti} = 0, T_e/T_i = 2, $a/L_n = a/L_{Te}$ = 3, υ = 0). For these conditions, the instability is the collisionless trapped electron mode (CTEM), with a mode frequency propagating in the electron diamagnetic drift direction. Also shown in Fig. 1 are |B| along a field line (middle) and the term proportional to the curvature drift (bottom). The eigenfunctions for these unstable TEMs are strongly localized in the low field, bad curvature region of the device, where the trapped particles exist. The structure of these instabilities is very similar to that observed in tokamaks, due to the quasisymmetric field.

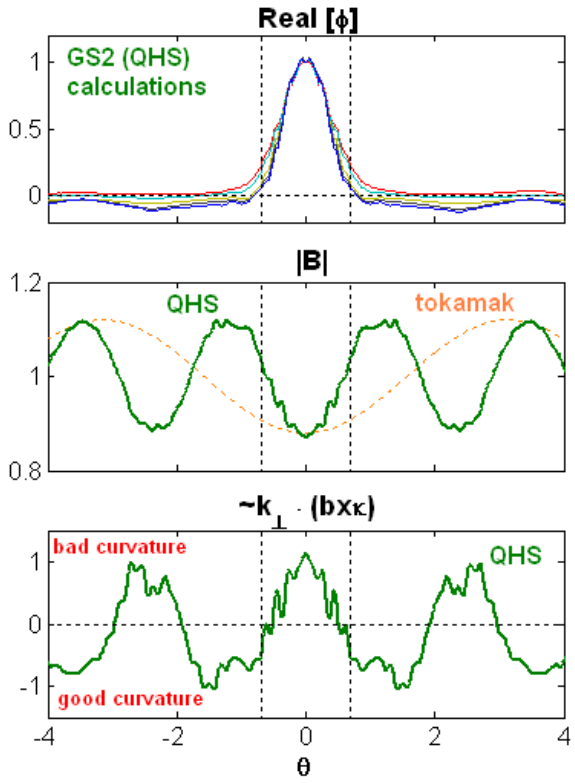

Fig.1 Normalized eigenfunctions (top), |B| (center), and curvature drift (bottom) for GS2 calculations in HSX.

3. 1D Predictive Transport Modeling

To model the anomalous particle and electron heat transport in HSX [19], the Weiland model [4] is utilized. The Weiland model is a toroidal fluid model for the ion temperature gradient (ITG) and TEM instabilities. It is a linearized set of equations that provides both linear stability predictions, and quasi-linear transport estimates of particle, and ion and electron heat transport. These transport estimates have been checked against a limited number of non-linear simulations [4,20] with good results. The Weiland ITG/TEM model forms the core of the Multi-Mode Model [21] used for numerous tokamak calculations.

As input, the Weiland model requires density and temperature gradient scale lengths (L_n, L_{Te}, L_{Ti}), temperature ratio (T_e/T_i), wavenumber ($k_\theta \rho_s$), trapped particle fraction (f_t), and a $\nabla B/\kappa$ scale length (L_B) to approximate the toroidal drift terms. In a tokamak, the trapped particle fraction is simply found using the toroidal ripple, $\varepsilon_T = r/R$, $f_t = \sqrt{2\varepsilon_T/(1+\varepsilon_T)}$, and the $\nabla B/\kappa$ scale length is the major radius, $L_B = R$.

To use the axisymmetric Weiland model for HSX, two approximations must be made to account for the local 3D geometry. These assumptions are based on the 3D gyrokinetic calculations discussed in Sec. 2. Since the unstable eigenmodes are strongly localized in the low field, bad curvature region (Fig. 1), the trapped particle fraction and $\nabla B/\kappa$ scale length are taken from this localized region of HSX. Because of the quasihelical symmetry, the trapped particle fraction is calculated using the dominant helical ripple ($\varepsilon_H = 0.14 \cdot r/a = 1.4 \cdot r/R$). In this location, where the axis undergoes an excursion to the outboard side, the local curvature is roughly three times larger than that of a tokamak with the same major radius. Therefore, the $\nabla B/\kappa$ scale length is reduced by a factor of three, $L_B = R/3$.

The Weiland model has been used with the above approximations to calculate the linear stability of HSX plasmas. Growth rates have also been calculated for the same input parameters using the 3D GS2 code for the QHS equilibrium. A comparison of growth rates is shown in Fig.

2 for a scan over density and electron temperature gradient, with the other parameters the same as in Fig. 1. As seen in the top two plots, the growth rates from the Weiland model are close in magnitude to the 3D GS2 calculations. For the range of gradients indicative of experiment (highlighted red lines) the agreement is better than 30%. If the local HSX geometry approximations are not used, the Weiland model underpredicts the growth rates by about a factor of two (Fig. 2, bottom).

In order to predict density and temperature profiles, 1-D flux surface averaged transport equations for electron density and temperature are solved numerically (Eqs. 1).

$$\frac{\partial}{\partial t}n+\frac{1}{V'}\frac{\partial}{\partial \rho}V'\left(-D\frac{\partial n}{\partial \rho}\left\langle|\nabla\rho|^2\right\rangle+V^{(n)}n\left\langle|\nabla\rho|\right\rangle\right)=\sum S(\rho) \qquad (1a)$$

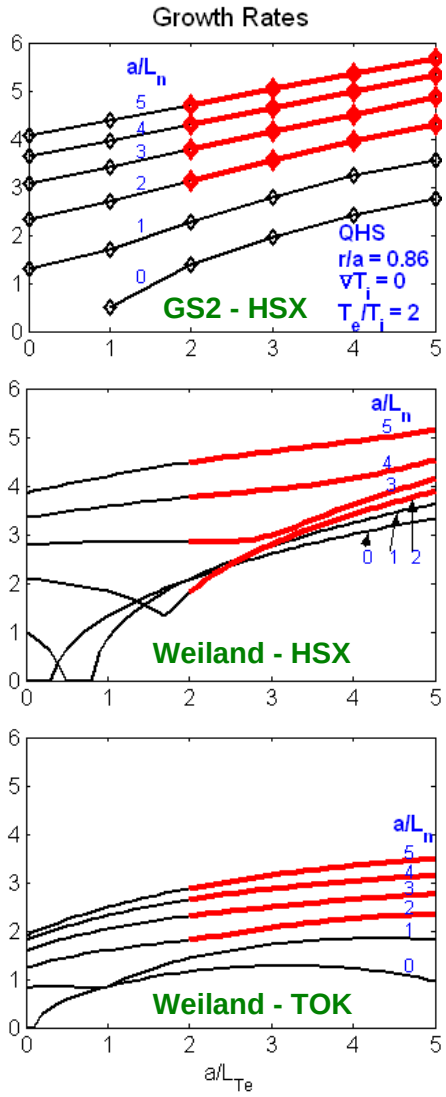

Fig.2 Growth rates (10^5 s^{-1}) calculated in HSX using 3D GS2 (top), the Weiland model with geometry approximations (center), and the Weiland model without geometry approximations (bottom). The highlighted lines represent typical experimental gradients.

$$\frac{3}{2}n\frac{\partial}{\partial t}T+\frac{1}{V'}\frac{\partial}{\partial \rho}V'\left(-n\chi\frac{\partial T}{\partial \rho}\left\langle|\nabla\rho|^2\right\rangle+V^{(nT)}nT\left\langle|\nabla\rho|\right\rangle\right)=\sum\frac{1}{e}P(\rho) \qquad (1b)$$

A multi-mode model approach is used, summing transport from the Weiland model (with geometry approximations), neoclassical transport (calculated using DKES [22,23]), and a small transport contribution from a resistive ballooning mode model, as used in [21]. For the neoclassical and Weiland model, the transport components are represented by both diffusive (D,χ) and convective ($V^{(n)}$, $V^{(nT)}$) components. The ECRH power deposition profile is calculated using a ray-tracing code, and the total absorbed power is determined from the time response of the diamagnetic flux loop during ECRH turn off. The particle source rate profile used is based on 3D neutral gas calculations [19]. The total magnitude is adjusted to minimize the difference in predicted and measured densities, but is usually within a factor of two of the neutral gas calculations that have been scaled to match absolutely calibrated H_α measurements.

Using the above sources and transport models, Eqs. 1 are integrated to steady state. Figure 3 shows a comparison of predicted and measured electron density and temperature profiles (using Thomson scattering) for B=1.0T QHS plasmas for two different injected powers (P_{inj} = 44 & 100 kW, O1 ECRH). The density profiles agree very well across the entire minor radius. The temperature profiles agree outside a normalized minor radius of ρ = 0.3, but the model underpredicts the core temperature. For four different injected powers (including two cases not shown here), the rms deviation of the simulated and experimental density profile

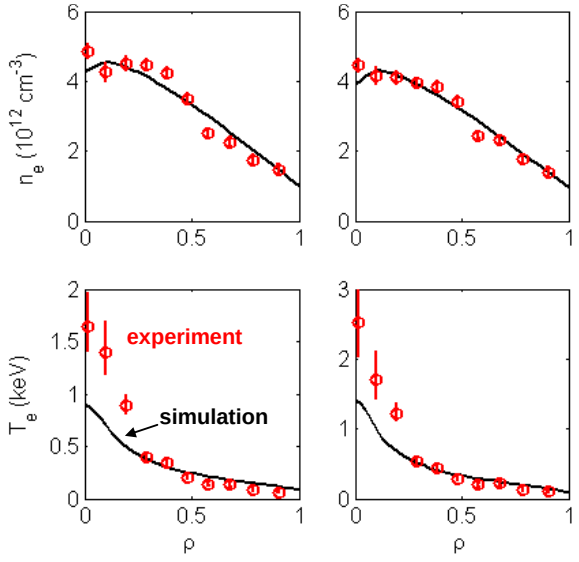

Fig.3 Predicted and measured electron density (top) and temperature (bottom) profiles for the QHS configuration for P_{inj} = 44 kW (left) and 100 kW (right).

($\sqrt{\sum\left(n^{sim}(\rho_j)-n_j^{exp}\right)^2}\Big/\sqrt{\sum\left(n_j^{exp}\right)^2}$, following ref. 3) is 9%. The rms deviation for T_e is considerably higher (40%).

The discrepancy of the core T_e profiles is due to a large χ_e from the Weiland TEM between ρ = 0.2-0.3, and a large neoclassical χ_e as the magnetic axis is approached. It is of interest to note that in the region between ρ = 0.2-0.3, the radial electric field predicted from the neoclassical ambipolarity constraint varies rapidly due to a change from the ion root to the electron root as the hot core is approached. In this region, estimated E×B shear rates [24] are larger than the linear TEM growth rates predicted from the transport modeling. This may indicate that E×B shear suppression could be important for determining the appropriate anomalous transport contribution.

Although the central T_e is not predicted with accuracy, the simulated energy confinement times agree within 10% of the experimental confinement times. Figure 4 shows the kinetic electron energy confinement times measured experimentally (red) and predicted by the simulations (blue) for four injected powers (26, 44, 70, 100 kW). The predicted confinement times scale like $\sim P^{-0.57}$, similar to empirical scaling laws [9] and to that expected from gyroBohm transport. Also shown are the energy confinement times determined from the diamagnetic measurements for similar line-averaged densities (black). These confinement times have a slightly weaker scaling with absorbed power, $\sim P^{-0.42}$.

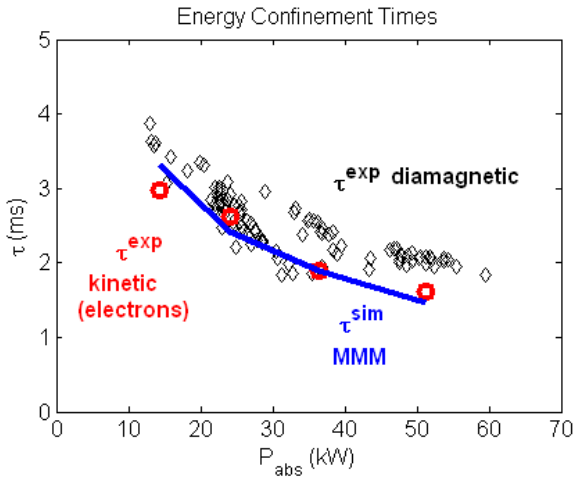

Fig.4 Predicted (blue) and experimental (red) kinetic energy confinement times. Also shown are confinement times from diamagnetic measurements only (black).

4. Conclusions

The Weiland ITG/TEM anomalous transport model has been used to predict transport in the HSX stellarator. By using approximations to represent the local geometry in HSX, the Weiland model predicts linear growth rates that agree within 30% of those calculated using the 3D gyrokinetic code GS2. Although non-linear effects or E×B shear suppression have not been included, the linear scaling should be captured reasonably well by this approximation. Predicted density profiles and energy confinement times (using the Weiland model plus appropriate neoclassical calculations) agree within 10% of experimentally measured values. Root mean square deviations in the electron temperature profile are larger (40%) due to a systematic underprediction of the core T_e.

References

[1] H.E. Mynick, Phys. Plasmas **13**, 058102 (2006).
[2] H. Yamada et al., Nucl. Fusion **41**, 901 (2001).
[3] ITER Physics Basis, Ch. 2 Nucl. Fusion **39**, 2175 (1999).
[4] H. Nordman et al., Nucl. Fusion **30**, 983 (1990).
[5] M. Kotschenreuther et al., Phys. Plasmas **2**, 2381 (1995).
[6] R.E. Waltz et al., Phys. Plasmas **4**, 2482 (1997).
[7] J.E. Kinsey et al., Phys. Plasmas **12**, 052503 (2005).
[8] A.J. Wooton et al., Plasma Phys. Contr. Fusion **34**, 2023 (1992).
[9] U. Stroth et al., Nucl. Fusion **36**, 1063 (1996).
[10] P. Xanthopoulos et al., Phys. Rev. Lett. **99**, 035002 (2007).
[11] T.-H. Watanabe et al., Nucl. Fusion **47**, 1383 (2007).
[12] M. Kotschenreuther et al,. Comp. Phys. Comm. **88**, 128 (1995).
[13] E.A. Belli et al., Bull. Am. Phys. Soc. **46**, No. 8, 232 (2001).
[14] S.P. Hirshman & D.K. Lee, Comp. Phys. Comm. **39**, 161 (1986).
[15] S.P. Hirshman et al., J. Comp. Phys. **87**, 396 (1990).
[16] D.V. Anderson et al., Int. J. Supercomp. Appl. **4**, 34 (1990).
[17] W.A. Cooper, Plasma Phys. Contr. Fusion **34**, 1011 (1992).
[18] G. Rewoldt et al., Phys. Plasmas **12**, 102512 (2005).
[19] J.M. Canik et al., Phys. Rev. Lett. **98**, 085002 (2007).
[20] A. Dimits et al., Phys. Plasmas **7**, 969 (2000).
[21] G. Bateman et al., Phys. Plasmas **5**, 1793 (1998).
[22] S.P. Hirshman et al., Phys. Fluids **29**, 2951 (1986).
[23] W.I. van Rij & S.P. Hirshman, Phys. Fluids **B** 1, 563 (1989).
[24] T.S. Hahm, Phys. Plasmas **4**, 4074 (1997).